Engineered Cardiac Tissue Microsphere Production through Direct Differentiation of Hydrogel-encapsulated Human Pluripotent Stem Cells

Ferdous B. Finklea[1], Yuan Tian[1], Petra Kerscher[1], Wen J. Seeto[1], Morgan E. Ellis, Elizabeth A. Lipke[*]

[1] Authors contributed equally

* Corresponding author

Department of Chemical Engineering, Auburn University, Auburn, AL 36849, United States

(E-mail: elipke@auburn.edu)

Keywords: PEG-fibrinogen, photocrosslinking, stem cell derived cardiomyocytes, engineered heart tissue, microsphere, scale-up, microfluidic encapsulation

Abstract

Engineered cardiac tissues that can be directly produced from human induced pluripotent stem cells (hiPSCs) in scalable, suspension culture systems are needed to meet the demands of cardiac regenerative medicine. Here, we demonstrate successful production of functional cardiac tissue microspheres through direct differentiation of hydrogel encapsulated hiPSCs. To form the microspheres, hiPSCs were suspended within the photocrosslinkable biomaterial, PEG-fibrinogen (25 million cells/mL) and encapsulated at a rate of 420,000 cells/minute using a custom microfluidic system. Even at this high cell density and rapid production rate, high intra-batch and batch-to-batch reproducibility was achieved. Following microsphere formation, hiPSCs maintained high cell viability and continued to grow within and beyond the original PEG-fibrinogen matrix. These initially soft microspheres (<250 Pa) supported efficient cardiac differentiation; spontaneous contractions initiated by differentiation day 8, and the microspheres contained >75% cardiomyocytes (CMs). CMs responded appropriately to pharmacological stimuli and exhibited 1:1 capture up to 6.0 Hz when electrically paced. Over time, cells formed cell-cell junctions and aligned myofibril fibers; engineered cardiac microspheres were maintained in culture over 3 years. The capability to rapidly generate uniform cardiac microsphere tissues is critical for advancing downstream applications including biomanufacturing, multi-well plate drug screening, and injection-based regenerative therapies.

Keywords: PEG-fibrinogen, photocrosslinking, stem cell derived cardiomyocytes, engineered heart tissue, scale-up, microfluidic

Introduction

Cardiovascular disease is the leading cause of death worldwide due to the limited ability of damaged myocardium to efficiently regenerate [1, 2]. It has been estimated that billions of cardiac muscle cells, cardiomyocytes (CMs), will be needed for cell therapy to be effective in treating myocardial disease [3]. Because of the inability to culture and expand adult CMs, stem cell-derived cardiomyocytes (SC-CMs) are a critical cell source for prevention and treatment of human cardiovascular disease [4]. Human induced pluripotent stem cells (hiPSCs) provide an option for production of specialized cells, such as cardiomyocytes (CMs), that are difficult to obtain from native tissue and cannot be cultured long-term *in vitro* [5, 6]. Therefore, further advancements in the scalable production of SC-CMs are needed to revolutionize their application in regenerative medicine, including treatment of heart failure patients, preclinical drug-testing, and studying disease mechanisms while overcoming interspecies and donor variation.

Currently 2D hiPSC monolayers are widely utilized for CM differentiation [7, 8]; however, this approach requires large surface areas, inherently limiting its scalability. Multiple emerging strategies employ suspension culture and differentiation of hiPSCs for scalable production of CMs, as recently reviewed by Kempf *et al* [9]. In particular, bioreactor-based formation of self-aggregated hiPSC embryoid bodies (EBs) is advantageous because of the single step approach, scalability, and elimination of the need for microcarrier removal [10-12]. Although these strategies possess great potential, efficiency of cardiac differentiation between pluripotent stem cell lines and even between batches of the same line can be highly variable [13-16]. Furthermore, the size and shape of EBs can be difficult to control and the self-aggregation process is shear rate dependent and lacks control over the resulting cell density and cellular microenvironment. Incorporating hiPSCs within a photocrosslinkable biomaterial can be used to enhance initial spheroid uniformity,

provide a homogeneous cellular microenvironment, guide stem cell differentiation, and provide localized physiological and biochemical cues to cells. Biomaterials have tunable mechanical, chemical, and biological properties as well as the ability to provide protection from shear stress, justifying their use in CM production from hiPSCs.

To meet the needs for bioreactor-based hiPSC-CM production, encapsulation materials must be degradable, while still providing the consistency, ease and speed of handling necessary for commercial scale-up. Natural biomaterials, including Matrigel [17], collagen, gelatin [18], alginate [19, 20], and fibrin [21] have long been used for formation of engineered cardiac tissue post-hiPSC differentiation, but have inherent limitations for use in rapid cell encapsulation and bioreactor culture. Incorporating a synthetic component to create a hybrid biomaterial overcomes these challenges, providing a reproducible, rapidly photocrosslinkable, and tunable microenvironment [22]. Previously, the hybrid biomaterials — poly(ethylene glycol)-fibrinogen (PEG-fibrinogen) and gelatin methacryloyl (GelMA) — have proven successful in the encapsulation and direct differentiation of hiPSCs to form 3D cardiac tissues [23, 24]. These materials provide essential structural and biological components necessary for the production of 3D cardiac tissues from hiPSCs [25] while enabling rapid photocrosslinking, which is necessary for scale-up and automatable process development.

Generation of 3D engineered cardiac tissues for use in regenerative medicine and drug-testing applications typically involves dissociation of CMs into single cells for further processing and assembly [26]. This requirement for CM dissociation creates challenges for cardiac tissue production and clinical translation due to the loss of cells and disruption of cell-cell junctions caused by the multiple cell-handling steps and the need for complex instrumentation and protocols. Rather than assembling tissues using pre-differentiated CMs, stem cell encapsulation and

subsequent direct differentiation within supporting biomaterial scaffolds provides an alternative approach for reproducible and scalable production of functional human cardiac tissue and can eliminate multiple cell-handling steps that otherwise limit the potential for process automation and production scale-up.

Previously, our group produced 3D cardiac tissues through hiPSC encapsulation and direct differentiation in PEG-fibrinogen [23] and GelMA [24] microislands. Whereas there are multiple advantages to this platform over 2D monolayer differentiation, including observation of T-tubule formation [23] and the use of a clinically relevant material [27], the microisland tissue geometry is not the optimal shape for use in suspension bioreactor culture, high-throughput drug screening, or injectable cell therapy. Therefore, to translate our approach to meet these needs, we have established a microfluidic system to rapidly encapsulate hiPSCs in hydrogel microspheres using a modified microfluidic oil-and-water emulsion technique.

Here we describe our results producing functional cardiac tissue microspheres through direct differentiation of encapsulated hiPSCs within a PEG-fibrinogen hydrogel in a single unit operation. Our custom microfluidic system can produce approximately 45 hiPSC microspheres per minute with a cell density of 25 million cells mL^{-1}, an approximate diameter of 900 μm, and tight control over roundness. Encapsulated hiPSCs remained viable in a PEG-fibrinogen hydrogel and continued to proliferate and grow to form larger and denser microspheres. Microspheres consistently showed initial areas of contraction on day 8 of differentiation, with high cardiac differentiation efficiency and reproducibility by day 10. Engineered cardiac microspheres showed appropriate functional responses to pharmaceutical stimuli isoproterenol and propranolol. Furthermore, microsphere CMs responded to outside pacing frequencies up to 6.0 Hz. Microspheres developed cell-cell junctions and displayed aligned myofibrils (day 60) and were

maintained in culture long-term (over 3 years). These results demonstrate our ability to reproducibly fabricate hiPSC-laden microspheres in an automatable and scalable manner with high CM yield and functionality, necessary for future applications in cell-therapy.

Materials and Methods

HiPSC expansion and maintenance

IMR-90 Clone 1 and 19-9-11 cell lines were obtained from WiCell. The hiPSC line SCVI55 was obtained from Joseph C. Wu MD, PhD at the Stanford Cardiovascular Institute, and the cell line, Un-Arc 16 Facs II [28], was graciously provided by Dr. Lior Gepstein at Technion – Israel Institute of Technology. HiPSCs were cultured on hESC qualified Matrigel (Corning) using mTeSR-1 medium (Stem Cell Technologies) or E8 and passaged into cell clusters using Versene (Invitrogen). E8 media consisted of ascorbic acid (64 mg/L, Sigma), sodium selenite (14 μg/L, Sigma), sodium bicarbonate (543 mg/L, Sigma), insulin (20 mg/L, Sigma), transferrin (10.7 mg/L, Sigma), basic fibroblast growth factor (100 μg/L, Peprotech), and transforming growth factor beta (2 μg/L, Peprotech) in DMEM/F12 (Gibco). For 24 *h* after passaging, hiPSCs were maintained in mTeSR-1 (IMR90, 19-9-11, UA16F2) or E8 (SCVI55) medium supplemented with ROCK inhibitor (5-10 μM, RI, Y-27632, Stem Cell Technologies).

PEG-fibrinogen synthesis

All chemicals were purchased from Sigma-Aldrich unless specified otherwise. Poly(ethylene glycol)-diacrylate (PEGDA) was formed by acrylating PEG (10 kDa) as described previously [29]. PEG-fibrinogen was prepared as previously described [30]. Briefly, bovine fibrinogen (300 mg) was dissolved in PBS with 8 M urea and tris (2-carboxyethyl) phosphine hydrochloride (TCEP-HCl, 22.53 mg) was added to the fibrinogen solution (7 mg mL^{-1}). Next, PEGDA (1.9392 g) was

reacted with fibrinogen (4:1 molar ratio) for 3 *h*, precipitated in acetone, and dissolved in PBS with 8 M urea. The reacted PEG-fibrinogen was dialyzed against PBS at 4 ºC for 24 *h*. To characterize the PEGylated product, fibrinogen content was measured using Pierce BCA assay (Thermo Scientific).

PDMS microfluidic device fabrication

The frame for fabricating the microfluidic device was made by 3D printing an acrylonitrile butadiene styrene bracket and then attaching a glass bottom and metal spacers to form the channels in the mold. The glass bottom was treated with Rain-X® for removal of the PDMS mold from the frame following curing of the PDMS. PDMS was synthesized using a Sylgard 184 silicone elastomer kit (Dow Corning) and poured into the frame, degassed, and cured at 60 °C for 2 *h*.

HiPSC microspheres production and cardiac differentiation

PEG-fibrinogen precursor solution was prepared by combining PEG-fibrinogen with triethanolamine (1.5 v/v%, TEOA), N-vinyl pyrrolidone (0.39 v/v%, NVP), and Eosin Y (0.1 mM, Fisher Scientific) photoinitiator (in PBS). HiPSCs were resuspended in PEG-fibrinogen precursor solution at 25 million cells mL^{-1}. The PEG-fibrinogen-cell mixture was added to one inlet of the custom-built microfluidic device. In parallel, mineral oil was added to the other inlet of the microfluidic device which, when combined with the PEG-fibrinogen-cell mixture, causes the formation of spherical droplets (**Figure 1a**). Flowrates for the PEG-fibrinogen-cell mixture and mineral oil were set at 1 mL h^{-1} and 10 mL h^{-1}, respectively. A light source (Prior) was used for photocrosslinking the liquid PEG-fibrinogen-cell mixture to form cell-laden microspheres. Microspheres were collected by washing down with mTeSR-1 medium, removed from the oil

phase and spent media, and cultured in mTeSR-1 medium + RI (5-10 μM) for 24 *h* (day -3). Microspheres were then cultured for an additional 48 *h* in mTeSR-1 medium with daily media changes (days -2 and -1).

Three days after microsphere production (day 0), cardiac differentiation [8] was initiated by changing medium from mTeSR-1 to RPMI/B27 minus insulin (4 mL, RPMI/B27-I, Thermo Fisher) supplemented with CHIR (10-12 μM, Stem Cell Technologies) per well. On day 1 (24 *h* after CHIR addition), medium was changed to RPMI/B27-I (4 mL). 48 *h* after that (day 3), 2 mL old media was combined with 2 mL fresh RPMI/B27-I supplemented with IWP2 (5 μM, Stem Cell Technologies). On day 5, media was replaced with RPMI/B27-I (4 mL) and on day 7, RPMI/B27-I was changed to RPMI/B27 medium (Thermo Fisher). RPMI/B27 medium was replaced every three to four days following differentiation.

Self-aggregated EB formation and cardiac differentiation

To form the self-aggregated EBs (day -3), hiPSCs were dissociated using Versene and collected in a single-cell suspension. One million cells were added to 4 mL of mTeSR + RI (5 μM) in a 6-well plate and placed on a shaker plate (Infors) at 70 rpm in a 5% CO_2 incubator. EBs formed overnight, and daily media changes occurred prior to initiation of cardiac differentiation on day 0. Cardiac differentiation followed the same protocol as the microspheres.

Microsphere diameter, roundness, and early growth quantification

Daily phase contrast images of microspheres were taken from the time of encapsulation (day -3) until initiation of cardiac differentiation (day 0). Microsphere diameter and size of eight individual batches were determined 24 *h* after encapsulation. Autofluorescence of the photoinitiator Eosin Y

in PEG-fibrinogen microspheres was captured using long acquisition times with the FITC filter on a fluorescence microscope at low magnification. Images were analyzed using ImageJ with standard plugins.

Microsphere growth prior to the initiation of spontaneous contraction was determined by analyzing phase contrast images on days -3, 0, 3, and 7 of differentiation by manual outlining of microspheres using ImageJ (n = 10).

HiPSC viability and immunofluorescence staining

24 *h* after encapsulation, hiPSC viability within PEG-fibrinogen microspheres was assessed using a LIVE/DEAD® viability kit (Invitrogen) and images were taken using a fluorescent microscope (Nikon). Alexa Fluor 568-Phalloidin (Invitrogen) was used as described by the manufacturer's protocol to visualize actin filaments in encapsulated cells. Whole, dissociated, or sectioned cell-laden microspheres were immunostained with Ki67 (Abcam), α-sarcomeric actinin (αSA, Sigma Aldrich), cardiac troponin T (cTnT, Invitrogen), and connexin 43 (Cx43, Sigma Aldrich). Microspheres were first rinsed with PBS and fixed in paraformaldehyde (4%, Electron Microscopy Sciences) or ice-cold acetone/ethanol (50/50) (Cx43) for 20 min at room temperature (RT) or -20 °C, respectively. Samples were rinsed with PBS and blocked with FBS (3%) overnight at 4 °C or 1 *h* at RT. Then, the cardiac microsphere samples were incubated in primary antibodies overnight at 4 °C or 1 *h* at RT followed by the addition of Alexa Fluor 488 and Alexa Fluor 568 secondary antibodies. Nuclei were counterstained with 4',6-diamidino-2-phenylindole (DAPI, Molecular Probes) or Bisbenzimide Hoechst 3342 (MilliporeSigma). All samples were visualized using a Nikon A1R laser-scanning confocal microscope.

DNA quantification

The DNA was quantified using a DNA Quantification Assay (Sigma-Aldrich) according to the manufacturer's instructions utilizing bisbenzimide H 33258 (Hoechst 33258). Individual microspheres were dissociated in Collagenase-B (1 mg/mL in PBS) for 10 minutes at 37 °C and resuspended in bisbenzimide H 33258 solution (1 μg/mL) for measurement on a plate reader (BIO-TEK Synergy HT). The data is reported as the mean ± standard deviation of 5 individual batches with a minimum of 2 microspheres per batch at each timepoint.

Cryosectioning

Microspheres were frozen and sectioned using a Microtome Cryostat HM 505E for immunostaining. The microspheres were embedded within Optimal Tissue Cutting Compound (TissueTek) in a square dish and frozen in methylbutane (EMD) that was kept cold using liquid nitrogen for 15-20 *s*. The frozen blocks were stored at -80 °C until sectioned. The cryostat was used to cut the blocks into 100-200 μm sections which were added to positively charged slides. The sections were then used for immunostaining and confocal imaging.

XTT assay

To verify hiPSC proliferation within PEG-fibrinogen hydrogels after encapsulation, cell activity on days -2 and -1 were determined using XTT assay (Biotium). One microsphere was placed in each well of a 96-well plate. Media was combined with XTT working solution and the well plate was incubated for 18 *h* at 37 °C; following incubation, the absorbance was measured using a Microplate Reader (Biotek).

Microsphere cardiomyocyte dissociation

Microspheres were washed with PBS followed by the incubation in dissociation solution containing collagenase type 2 (1 mg mL^{-1}, Worthington) at 37 °C for 2 *h* or Collagenase B (Sigma-Aldrich) for 10 min. The dissociation solution contained NaCl (120 mM), KCl (5.4 mM), $MgSO_4$ (5 mM), Na-pyruvate (5 mM), glucose (20 mM), taurine (20 mM), and HEPES (10 mM, pH 6.9) supplemented with $CaCl_2$ (30 μM) and ROCK inhibitor (5 μM). Microspheres were centrifuged, resuspended in trypsin EDTA (0.25%, Corning) and incubated at 37 °C for 5 min. Trypsin was neutralized using RPMI20 (FBS (20%) in RPMI1640 medium); cells were resuspended in RPMI20 with ROCK inhibitor (5 μM). Dissociated cells were plated on fibronectin coated (25 μg mL^{-1}, ThermoFisher) substrates (PDMS-coated glass coverslips or MEA) and incubated for three days.

Scanning electron microscopy

For SEM, microspheres were rinsed with PBS and fixed in paraformaldehyde (4%) and glutaraldehyde (2%) in PBS for 15 min. The microspheres were rinsed with PBS and then osmium tetraoxide (2%) was added for 1.5 *h*. After further PBS rinses, the microspheres were flash frozen using liquid nitrogen and then lyophilized. Dried microspheres were mounted on aluminum stubs, sputter-coated with gold (Pelco SC-6 sputter coater) and imaged using JEOL JSM-7000F scanning electron microscope.

Parallel plate mechanical testing

Day -2, 5, 8, and 17 microspheres were compressed using a micron-scale mechanical testing system (Microsquisher, CellScale) [31] to determine their mechanical properties using a Tungsten cantilever beam (modulus = 411 GPa, diameter = 203.2 μm). All microsphere samples were

analyzed in PBS at 37 ºC. Young's modulus was calculated at 10% deformation using the previously published method [32]. The force at 10% deformation was determined from a linear regression of force versus displacement (n = 8 microspheres per condition).

cDNA synthesis and RT-qPCR

RNA was isolated using a Nucleospin RNA XS kit (Machery-Nagel) from hiPSC microspheres as well as engineered cardiac microspheres on day 10, 20, and 30. Tissues were frozen in liquid nitrogen and stored at -80 °C until time for analysis. The cells were thawed and lysed by vortexing. The lysate was filtered to remove large cell particles and debris. The RNA was bound to the RNA XS column and the DNA was digested using a DNase. After a series of washes, the pure RNA was eluted and collected. The concentration of the RNA was determined using a NanoDrop 1000 UV-Spectrophotometer (ThermoFisher).

A SuperScript III Platinum One-Step RT-qPCR kit (Invitrogen) was used for qPCR analysis with 25 ng of RNA sample. A Bio-Rad CFX96 thermal cycler was used to run the samples at 50 °C for 15 min for cDNA synthesis followed by a 95 °C incubation for 3 mins. The genes of interest were amplified using 45 cycles 95 °C for 15 *s* followed by 55 °C for 30 *s*. Detection of amplification was done using Taqman probes along with forward and reverse primers (**Supplementary Table 2**). Three biological replicates were analyzed in duplicate for each time point. The fold change in gene expression was determined from the $2^{-(\Delta Ct)}$ method in which ΔCt is the difference between the Ct from the sample and Day 10 Ct (or hiPSCs for Oct4). Statistical analysis was performed on the Ct values using a one-way ANOVA with Tukey's test for post-hoc analysis for samples with

equal variance, and Games-Howell test for samples with unequal variances. A value of $p < 0.05$ was used for statistical significance.

Flow cytometry

After tissue dissociation, a cell pellet was collected through centrifugation. After washing with PBS, the cells were labeled with Zombie Dye (Biotium) for 30 min at 4 °C. Cells were then washed with Blocking Buffer (bovine serum albumin (1%, BSA, Sigma), fetal bovine serum (10%, FBS, Atlanta Biologics) in PBS), and then fixed with Foxp3 Transcription Factor Staining Buffer Set (eBioscience) overnight at 4 °C. The cells were then filtered using a 70 μm cell strainer (Scienceware Flowmi) and permeabilized with FACS buffer (BSA (1%), FBS (10%) in 1x Permeabilization Buffer (eBioscience)) at RT for 30 mins. The primary antibodies (cTnT (1:400, Invitrogen), MF20 (1:200, DSHB), TE-7 (1:100, Sigma), MYL11 (1:100, Sigma), PDGFRα (20 μL/1x10^6 cells, BD), Ki67 (1:200, Abcam), and/or P4HB (1:200, Abcam)) were then incubated with the cells for 1 *h* at RT or 4°C overnight. After incubation in the primary antibody, washing occurred with Permeabilization Buffer. The secondary antibodies (1:300, AlexaFluor 488 goat anti-rabbit IgG and AlexaFluor 647 goat anti-mouse IgG (ThermoFisher)) were added for 30 mins at RT. The cells were then washed with Permeabilization Buffer and resuspended in Blocking Buffer for analysis. An Accuri C6 or Beckman Coulter CytoFlex LX was used for sample analysis. At least 10,000 cells were recorded for analysis. Isotype controls (Anti-Mouse IgG1 and Anti-Rabbit IgG (ThermoFisher)) were used to ensure there was not any non-specific binding.

Masson's Trichrome Staining

Microspheres were fixed in Bouin's fixative for 1 h, washed with water three times for 10 min each, 70% ethanol two times for 10 min each, 80% ethanol for 10 min, 95% ethanol for 10 min, 100% ethanol two times for 5 min, and 3 times with XS-3 (StatLab); all washing steps were done with agitation. Microspheres were paraffin embedded, sectioned at a thickness of 5 μm, and heated in a 58°C oven for 10 min. Masson's trichrome staining (Poly Scientific R&D) was performed according to the manufacturer's instructions. Microsphere sections were imaged using a ScanScope CS (Leica).

Multielectrode array

Day 20 and 50 dissociated microsphere CMs were seeded onto a fibronectin coated S2 type MEA200/30-Ti-gr (Multichannel Systems) and cultured for at least 24 h. Adhering microsphere CMs were perfused with Tyrode's solution, composed of $CaCl_2$ (1.8 mM), glucose (5 mM), HEPES (5 mM), $MgCl_2$ (1 mM), KCl (5.4 mM), NaCl (135 mM), and NaH_2PO_4 (0.33 mM) at pH 7.4 and 37 ºC. Once stabilized, field potentials of spontaneous contractions were recorded at a sampling frequency of 10 kHz. Drug response of day 20 microsphere CMs was tested by adding the β-adrenergic agonist isoproterenol (1 μM) and antagonist propranolol (1 μM). Day 50 microsphere CMs were exogenously paced from 0.5-6.0 Hz.

Optical mapping of calcium transients

A high-speed camera (Andor iXon+ 860 EMCCD) was used to take calcium recordings of at least 1600 pixels of plated engineered cardiac tissue microspheres using our previously established optical mapping system [33]. The cardiomyocytes were stained with Rhod-2 AM dye (5 μM, Invitrogen) with Pluronic F-127 (0.02%) in Tyrode's Solution for 30-120 min with blebbistatin

(10 μM, EMD). Tyrode's solution was prepared by combining calcium chloride (1.8 mM) and glucose (5.0 mM) with HEPES (5.0 mM), magnesium chloride (1.0 mM), potassium chloride (5.4 mM), sodium chloride (135 mM), and sodium phosphate (0.33 mM) and adjusting the pH to 7.4 with sodium hydroxide. Warm Tyrode's Solution was perfused through the optical mapping chamber before adding the sample. The plated engineered cardiac tissue microspheres were added to the chamber and recordings were taken with and without electrical pacing. A custom MATLAB script was used for analysis in which the change in fluorescence was used to calculate the calcium transient duration (CTD) at each location in a recording.

Statistical Analysis

Unless otherwise noted, statistical analysis was performed using Minitab statistical software where results are presented as mean ± standard deviation. One-way ANOVA was performed with Tukey's test for post-hoc analysis for samples with equal variance, and the Games-Howell test was performed for samples with unequal variances. A value of $p < 0.05$ was used for statistical significance.

Results

Rapid, one-step microfluidic encapsulation system produced uniform hiPSC microspheres

A microfluidic cell-encapsulation system was developed to rapidly produce uniform spherical hydrogels using a modified microfluidic oil-and-water emulsion technique (**Supplementary Figure 1**, **Supplementary Movie 1**). The central component of the system is a device made of polydimethylsiloxane (PDMS), which has two inlets, an outlet, and a modified T-junction (**Figure 1a**). Within this system, a suspension of hiPSCs in aqueous PEG-fibrinogen precursor solution —

the discrete phase — was pumped through the top inlet of the PDMS microfluidic device. In parallel, mineral oil — the continuous phase — was pumped through the bottom inlet of the device; the two inlet streams come together at the device T-junction. Microspheres were formed through emulsification and traveled through the perpendicular outlet channel where they were photocrosslinked. Crosslinking occurred rapidly, with a light exposure time of 1.6 seconds per microsphere, and crosslinked microspheres were collected from the end of the outlet channel using a continuous downward flow of cell culture media, removed from the oil phase and washing media, and transferred to a well-plate.

Encapsulation of hiPSCs occurred on day -3 of cardiac differentiation. Following encapsulation, hiPSCs (25 x 10^6 cells mL^{-1} PEG-fibrinogen) maintained high viability **(Figure 1b**, **Supplementary Movie 2)**, and as a result of the high cell density, hiPSCs were tightly packed throughout the microsphere, displaying a round morphology with some cells being exposed beyond the PEG-fibrinogen hydrogel boundary (**Figure 1f**). Approximately 45 hiPSC microspheres were produced per minute with tight control over size and roundness (**Figure 1c-e**). Each microsphere contained approximately 9500 hiPSCs; this equates to an encapsulation rate of 420,000 cells min^{-1}. Therefore, a clinically relevant number of cells, 8 million, as used in our previous large animal wound healing study [34] can be encapsulated using this system in less than 20 minutes, and enough spheres to fill a 384-well plate for high-throughput screening assays can be produced in less than 10 minutes with one microfluidic device.

This microfluidic system reproducibly produced uniform microspheres with highly consistent size and shape not only within a batch, but also between batches. For 8 batches, the average diameter of the microspheres ranged from 850 – 952 μm and the average roundness was above 0.933 with low variance within a batch (diameter coefficient of variance (CV) < 10%,

roundness CV < 5%, $n \geq 32$ microspheres per batch, **Supplementary Table 1**). Furthermore, variance between batches was also low; on the day of encapsulation (day -3, **Figure 1c**), average initial microsphere diameter was 908 ± 40 μm (CV = 4.4%, **Figure 1d**) and roundness was 0.956 ± 0.02 (CV = 2.1%, **Figure 1e**, $n = 8$ independent batches).

HiPSC microspheres continued to proliferate and grow prior to initiation of cardiac differentiation. Following encapsulation (day -3), cells first grew within the original hydrogel boundaries, maintaining the initial microsphere diameter. Encapsulated hiPSCs were evenly distributed within the PEG-fibrinogen hydrogels (**Supplementary Movie 3**) with high cell density throughout the microspheres as shown by immunofluorescent labeling of the nuclei in cryosections (**Figure 1g)**. HiPSCs were cultured in their pluripotent state for three days before cardiac differentiation was initiated on day 0 (**Figure 1)**. Previously we found that three days was sufficient for hiPSCs to adapt to their new 3D hydrogel microenvironment and initiate cell growth within the hydrogel, forming a continuous tissue over time [23, 24]. HiPSC microspheres behaved similarly, occupying the majority of the spherical volume by day 0 (**Figure 1f**).

Encapsulated hiPSCs grew to form continuous cell-laden microspheres

After initiation of cardiac differentiation (day 0), the cells continued to grow within and then beyond the initial microsphere boundaries to produce denser and larger tissues with decreasing roundness (**Figure 2a**). For two different lines of encapsulated hiPSCs, IMR90 and 19-9-11, XTT assay results confirmed higher metabolic activity on day -1 than on day -2 ($n = 5$ microspheres, **Figure 2b**), which combined with visual phase contrast data (**Figure 2a**) and Ki67 staining (**Figure 2c**), confirms an increase in the number of viable and proliferative cells. By differentiation day 3, microsphere diameter had increased by a factor of 1.27 ± 0.22 when compared to day 0 and

had further increased to 1.7 ± 0.11 times by day 7 (n = 10, **Figure 2d**, **Supplementary Figure 2a-b**). The total number of cells increased throughout differentiation with a significantly higher number of cells by day 7. The number of cells per encapsulated hiPSC on day -3 was 0.96 ± 0.55, 1.43 ± 0.70, and 2.8 ± 0.54 on days 0, 3, and 7 (n = 5 individual batches, **Supplementary Figure 2c**). Additionally, the ratio of DNA on days 3 and 10 with respect to day 0 was 1.32 ± 0.49 and 1.40 ± 0.41, respectively (n = 5 individual batches, **Supplementary Figure 2d**).

One factor influencing stem cell differentiation is the mechanical stiffness of the cellular microenvironment. Typically, 2D monolayer cardiac differentiation of hiPSCs occurs on tissue culture polystyrene surfaces which are much stiffer (>1 GPa) than conditions during embryonic development (<100 Pa). Stiffness of cell-laden microspheres was assessed prior to and during differentiation using parallel-plate compression testing; the elastic modulus was 62 ± 28, 59 ± 32, 118 ± 32, and 103 ± 21 Pa, respectively, on days -2, 5, 8, and 17 (n = 8, **Figure 2g**), providing a more physiological microenvironment for the cells during differentiation. This temporal increase in tissue stiffness was accompanied by changes in cell morphology from round cell colonies on day 0 (**Figure 2e**) to elongated cells following differentiation (day 10, **Figure 2f**), indicative of cardiac differentiation.

Encapsulated hiPSCs differentiated into engineered cardiac tissue microspheres

HiPSC-laden microspheres were successfully differentiated into spontaneously contracting engineered cardiac tissue. Suspension cultured microspheres initiated spontaneous contractions by day 8 of differentiation, with approximately 78% of microspheres contracting by day 10 (n = 90 microspheres, **Supplementary Movie 4**). Differentiation efficiency on day 10 was consistently high between batches with approximately 75% total CMs (75.1 ± 6.7 % cTnT+, 75.2 ± 7.1 %

MF20+, *n* = 16 individual batches**, Figure 3a**, **Supplementary Figure 3**); this corresponds to efficiency previously achieved with our differentiation protocol [23] and hiPSC lines using 2D sheet differentiation [35] and is significantly higher than self-aggregated EBs using the same protocol (20.8 ± 19.3 % cTnT+, **Supplementary Figure 4a**). Further examination showed 3.3 ± 2.9% of the cells were positive for fibroblast marker, TE-7, 7.36 ± 5.75% were positive for cardiac fibroblast marker, PDGFRα, and 10.3 ± 2.7% were positive for smooth muscle marker, MYL11 (**Figure 3b**, **Supplementary Figure 3**); this indicates that the non-CM cell population was comprised mostly of fibroblasts and smooth muscle cells, similar to previously published work using this differentiation protocol [36]. Following differentiation, 5.8 ± 1.2 million CMs were obtained per batch yielding 2.0 ± 0.34 CMs per encapsulated hiPSC on day -3; although comparable cell numbers were obtained per batch in the EBs on day 10 (6.3 ± 1.4 million cells), only 1.4 ± 1.3 million of those cells were CMs, due in part to the large variability in differentiation efficiency. EB differentiation yielded 1.4 ± 1.3 CMs per hiPSC (**Supplementary Figure 4b-c**) with larger variability than in the engineered cardiac tissue microspheres. The cell population was maintained through at least day 20, with 71.6 ± 8.4% CMs, 7.1 ± 1.7% proliferative CMs (cTnT+/Ki67+), and 8.41 ± 6.5% of the cells positive for P4HB, a fibroblast marker (*n* = 3 individual batches, **Supplementary Figure 3a**). Cell density increased during cardiac differentiation from day 0 (initiation of differentiation, **Figure 1g**) through day 12 (**Figure 3c**). CM distribution and morphology in both whole microspheres and sections was observed through immunostaining for cardiac markers, cardiac troponin T (cTnT) and α-sarcomeric actinin (αSA), and functional protein Cx43 (**Figure 3c, i-k**). Sarcomere alignment and organization increased with progressing culture time, and engineered cardiac microspheres expressed gap junction protein, Cx43 (**Figure 3i-k**).

Microspheres displayed appropriate temporal expression of initially pluripotent and then later cardiac genes, which was quantified using RT-qPCR (primer sequences can be found in **Supplementary Table 2**). During cardiac differentiation, an expected decrease occurred in the expression of pluripotency gene, OCT4 (**Figure 3d**). Expression of MLC2v, a ventricular CM gene, and βMHC, a cardiac gene, significantly increased from day 10 to day 30 (**Figure 3e, g**). These results, along with an increase in the ratio of βMHC/αMHC expression from day 10 to day 30, are consistent with expression patterns during CM development and maturation. Expression of αMHC increased from day 10 to day 20 and then decreased from day 20 to 30 (**Figure 3f**). Additionally, days 10, 20, and 30 cardiac microspheres had similar expression of functional gap junction protein Cx43 (**Figure 3h**).

Engineered cardiac microspheres showed dynamic remodeling of their PEG-fibrinogen microenvironment

With progressing culture time, encapsulated cells completely remodeled their PEG-fibrinogen microenvironment and differentiated into maturing cardiac tissues. Examining sequential cryosections from microspheres in culture for over a year, cardiomyocytes were present throughout the entire cardiac tissue microsphere, based on positive αSA expression (**Supplementary Figure 5**); representative sections from the middle of the microsphere are shown in **Figure 4a-c**. ECT microspheres secreted extracellular matrix (ECM), including an increase in collagen deposition from day 28 (**Figure 4d**) to day 98 (**Figure 4e**) throughout the microsphere and around the edge (**Supplementary Figure 6**) as visualized by Masson's trichrome staining on cardiac microsphere sections (**Figure 4d-e)**. Some sections of the cardiac microspheres contained cells with highly organized structure and alignment, reminiscent of native cardiac tissue structure (**Figure 4f**).

Scanning electron microscopy (SEM) of microspheres showed a smooth cell-based surface (**Figure 4g**), demonstrating cellular remodeling of the matrix during cardiac differentiation (**Supplementary Figure 7**). At higher magnification, tightly-connected cells and ECM deposition were observed on the microsphere surface (**Figure 4h**). Day 120 microspheres showed aligned cells (**Figure 4h**) on the microsphere surface, with neighboring cells forming cell-cell junctions (**Figure 4i**). Additionally, day 60 microspheres appeared to have aligned myofibril arrangement (**Figure 4j**), similar to SEM images of native human heart tissue (**Figure 4k**) [37]. Understanding CM functionality and maturity on both a tissue and single-cell level is often desired. Engineered cardiac microspheres can be dissociated into single CMs, with CMs spontaneously contracting after dissociation (**Supplementary Movie 5**). CMs attached to unpatterned PDMS surfaces with elongated cell morphology, which is normal for maturing CMs [23]. Dissociated, plated CMs displayed defined sarcomere structures with internal alignment and length of 1.85 μm (**Figure 4l**) which falls between the range for fetal (1.8 μm) and adult (2.0 – 2.2 μm) CMs, and is greater than typical hPSC-CMs (1.6 – 1.7 μm); an organized sarcomere arrangement improves the mechanical contractile output and is indicative of cardiomyocyte maturation [38].

Microsphere CMs responded to drug treatment and electrical stimuli

For the successful translation of engineered cardiac tissues towards regenerative medicine and drug-screening applications, the appropriate response to pharmacological and electrical stimuli is essential. Response to these stimuli indicates functionality and maturity of the resulting CMs. Using a multielectrode array (MEA) (**Supplementary Movie 6**, **Figure 5a-c**), we evaluated the response of our day 20 engineered cardiac microspheres to pharmacologic stimuli including the β-adrenergic agonist, isoproterenol, and the β-adrenergic antagonist, propranolol. Isoproterenol

increases the frequency of contraction, while the subsequent addition of propranolol slowed down the rate of contraction (**Figure 5b**). In addition to drug-testing, we also investigated the response of engineered cardiac microspheres to electrical pacing. Day 50 microsphere CMs exhibited 1:1 capture up to 6.0 Hz when paced on the MEA (**Figure 5c**). Ion exchange of calcium, sodium, and potassium through the CMs is responsible for the contractile motion of these cells; a key difference between fetal and adult CMs is the rate at which ions are transported throughout the CMs. The calcium transients through plated engineered cardiac tissue microspheres were visualized using an optical mapping platform in which a calcium dye, Rhod-2, was employed to quantify the calcium transient duration (CTD) (**Supplementary Figure 8**). The CTD at 50% and 80% repolarization for these engineered cardiac tissue microspheres was 450 ms and 680 ms for samples paced at 1 Hz (n = 2 recordings) and 380 ms and 500 ms at 1.5 Hz, respectively (n = 3 recordings**, Figure 5d**). Contraction analysis was performed using a custom MATLAB script [39] in which videos were converted into a set of tiff files for macroblock tracing to detect the frequency of contraction as well as the contraction and relaxation velocities. Microspheres contracted at a frequency of 16.6 ± 5.9, 13.8 ± 2.3, and 25.6 ±1 0.8 beats per minute on days 20, 30, and 60 respectively ($n \geq 11$, **Figure 5e**). The contraction and relaxation velocities were 110 ± 49, 161 ± 69, and 175 ± 112 μm s^{-1} on days 20, 30, and 60 with relaxation velocities of 70 ± 36, 106 ± 42, and 146 ± 88 μm s^{-1}, respectively ($n \geq 11$, **Figure 5f);** a representative trace can be seen in **Figure 5g**. Appropriate response to drug treatment and electrical pacing, both on the MEA and in an optical mapping platform, along with increasing contraction and relaxation velocities indicate functionality of the resulting CMs within the engineered cardiac tissue microspheres.

Discussion

High-throughput production of 3D cardiac tissues is necessary for applications in drug-testing and clinical translation of regenerative therapies. Engineered cardiac tissue production must be reproducible, cost-effective, and scalable to become a viable treatment option for cardiovascular disease. Building on spherical CM production using self-aggregated EBs, here we have shown the ability to produce spheroidal tissues for hiPSC differentiation while simultaneously controlling the cellular microenvironment and tissue geometry through the incorporation of a cellular responsive biomaterial, PEG-fibrinogen. A custom microfluidic system has been implemented to rapidly encapsulate approximately 420,000 cells per minute, forming highly uniform hiPSC microspheres for direct differentiation into functional engineered cardiac tissue microspheres.

Following encapsulation using this microfluidic system, hiPSCs were evenly distributed throughout the PEG-fibrinogen microspheres and maintained high viability; cell density within the constructs began to increase shortly after encapsulation based on visual observation and metabolic activity analysis. Cell proliferation was observed throughout the time course of cardiac differentiation with cells initially filling the original hydrogel construct and then continuing beyond, resulting in tissue growth and a decrease in roundness of the tissues. Spontaneous contractions consistently started by day 8 of differentiation, and engineered cardiac tissue microspheres were composed of over 75% CMs on day 20, achieving similar efficiency to small molecule 2D monolayer differentiations using the same hiPSC lines and differentiation protocol [8]. Contraction and relaxation velocities increased over time and microsphere CMs responded appropriately to pharmacologic stimuli, including β-agonist, isoproterenol, and β-antagonist, propranolol. Furthermore, engineered cardiac microspheres exhibited 1:1 capture for external pacing up to 6.0 Hz. During culture, proliferating and differentiating cells remodeled their provided PEG-fibrinogen microenvironment while depositing their own ECM proteins. Results

demonstrate hiPSC differentiation, cardiac tissue formation, and electromechanical function of microsphere CMs, making this a promising cardiac tissue model for cell-therapy and drug-testing.

Production of spherical cardiac tissue structures has been studied for years, starting with self-aggregated EBs [14], the initial stem cell differentiation approach to form spontaneously contracting CMs. Successful EB cardiac differentiation relies on EB size and intercellular interactions; however, due to inherent variability in these processes, low CM differentiation efficiency and poor reproducibility can result [40]. To improve control, microwell plates [41, 42], centrifugation [43, 44], hanging droplet formation [45], and vortexing [46] have been used for production of more uniform cell-laden spheroids. However, these modified methods can be tedious, relatively low-throughput, and/or have a high potential for variability and low reproducibility between laboratories. Recent work in large-scale production of CMs has demonstrated that the formation of pluripotent stem cell aggregates from a single-cell suspension can be controlled by bioreactor culture system operating parameters [11]. This has proven successful for large-scale production of CMs, although optimization is still needed to obtain consistency in terms of CM yield and differentiation efficiency. In all cases, post-differentiation processing, consisting of CM dissociation and encapsulation within a biomaterial scaffold, is typically required to obtain a functional 3D engineered tissue.

By directly differentiating the hiPSCs within the PEG-fibrinogen matrix, we overcome the need for this post-differentiation processing, using a single cell-handling step for the formation of engineered tissues cardiac microsphere. PEG-fibrinogen is a hybrid biomaterial that is currently undergoing clinical trials for the repair of cartilage tissue [27]. The use of biomaterials in cell and tissue production offers an additional tool to overcome challenges inherent to self-aggregated hiPSC EB formation and cardiac differentiation and maturation. Biomaterials can be employed not

only to provide a controlled 3D supporting microenvironment [47], such as for a cardiac patch [36, 48], but also to protect encapsulated cells from shear in bioreactor culture or during injection [22, 34, 49-51]. Biomaterials can be used to manipulate multiple aspects of the cellular microenvironment including: guiding cell-cell and cell-material interactions through inclusion of cell adhesion and degradation sites, controlling cell density and engineered tissue size and shape, and recapitulating mechanical and biological cues present in the *in vivo* systems of interest [52-54]. Previous studies show biomaterials can promote consistency and drive CM phenotypical and functional maturation using nitric oxide [33], electrically conductive materials [55-57], patterning and topography [58, 59], and mechanical and electrical stimulation [60, 61]. We take advantage of material cues to provide uniformity to the initial stem cell microenvironment, support CM differentiation, and push CM maturity.

Recapitulating embryonic and fetal cardiac properties has been previously shown to be effective in driving cardiac tissue formation and maturation, particularly with regard to electrical stimulation [60]. Prior studies have shown that 2D substrates with similar stiffness to the native adult heart (10 kPa) are beneficial to enhancing CM function and maturation following cardiac differentiation [62, 63]. Developing cardiac tissues are much softer; the stiffness of chick embryo hearts increases 9-fold, from 900 Pa to 8.2 kPa, between 36 to 408 hours post-fertilization [62]. However, prior to germ layer specification during gastrulation, embryos are much softer than either the adult heart or developing cardiac tissues with elastic moduli reported as low as 5 Pa for frog embryonic tissue [64]; therefore, we hypothesize that a softer microenvironment, similar to that of an embryo, is critical for success of cardiac differentiation of hiPSCs within a biomaterial scaffold. Our results here demonstrating successful differentiation of CMs from hiPSCs within a PEG-fibrinogen matrix, as well as in our previous study within GelMA [24], support further

investigation of this relationship; in both cases, constructs with a low initial elastic modulus (less than 250 Pa) supported efficient cardiac tissue formation.

For engineered cardiac tissues to be useful for downstream applications such as regenerative medicine or drug screening, they must reasonably mimic the adult cardiac electrophysiology. Engineered cardiac tissues have potential to make an immediate impact on the improving preclinical testing of new drug candidates; current methods of preclinical testing rely on *in vitro* assays using oversimplified immortalized cell lines and *in vivo* small animal testing platforms. These do not reliably mimic human electrophysiology or accurately predict cardiotoxicity of newly developed drugs on the adult heart, resulting in large numbers of Phase I clinical trial failures and post-approval drug withdrawals from the market [65]. The ability to recapitulate adult cardiac electrophysiology and accurately predict cardiotoxicity *in vitro* would provide measurable cost and time saving benefits to the pharmaceutical industry [66]. In this study, we showed that our engineered cardiac tissue microspheres appropriately responded to exogeneous pacing up to 6 Hz and drug testing with β-adrenergic agonist, isoproterenol, and the β-adrenergic antagonist, propranolol. Furthermore, optical mapping showed an expected decrease in CTD with increased frequency of electrical pacing. The engineered cardiac microspheres maintained their spontaneous contractile phenotype in culture with velocity of contraction trending upward over time. These results show appropriate response to external stimuli, displaying features of maturing CMs and potential for use in *in vivo* studies for regenerative medicine and drug-testing. Our tissues do not fully recapitulate the mature adult CM phenotype; however, they fall within the range of other hiPSC-CM platforms [38, 67, 68], and further maturation may be achieved using external mechanical or electrical stimulation.

Once large quantities of CMs are produced for cell therapy, the engineered cardiac tissue must be successfully delivered and engraft to the infarcted myocardium, which has proven challenging; research has shown that direct injection of cardiac microtissues to the myocardium results in better CM retention and engraftment than delivery through intracoronary or intravenous injections or using an epicardial tissue patch [69, 70]. Pre-clinical studies infusing or transplanting hPSC-CMs [71-73] into the heart have shown cell-therapy can increase cardiac function; although mechanisms for these observed improvements are not yet fully understood, electrical coupling and engraftment, as well as paracrine signaling, are thought to be involved [17, 74, 75]. PSC-derived cardiac progenitor cells [76] or hPSC-CMs [72] have successfully been used alone and in combination with fibrin [77] or collagen [78] for small animal models and non-human primate trials. A human clinical trial using hPSC-derived cardiovascular progenitors has been initiated [79]; Dr. Menasche provides a detailed review on previous and ongoing cell therapy trials [80]. The microfluidic cell encapsulation system employed here has been previously used to encapsulate cells for injectable cell delivery in large animal pre-clinical wound healing studies [34]. The engineered cardiac tissue microspheres produced using the microfluidic encapsulation system and differentiation method established in this study hold promise for use in injectable cardiac cell therapy. Current studies are ongoing to increase efficiency of cardiac differentiation and clinical relevance through adaption of xeno-free cell production methods [7].

Uniform and precise 3D cell-material constructs can now be produced by emerging technologies including bioprinting [81-85] and microfluidic systems [34, 86-88]. The custom microfluidic system presented here can be used for scalable microsphere production that provides a reproducible 3D microenvironment while leveraging an EB-like differentiation approach. Currently in the field of tissue engineering, hydrogel-based microsphere size is limited to 100-

200 μm [86, 87, 89] due to standard soft-lithography fabrication techniques [90]; microspheres with larger diameters are often more difficult to produce with high uniformity and roundness. Stability constraints typically limit microfluidic systems to single cell encapsulation, and do not support encapsulation of small cell clusters, such as the post-dissociation hiPSCs employed here [91]. Testing has shown hiPSCs are sensitive to suspension in oil; therefore, the limiting light and oil exposure time were key factors during system design. In-line photocrosslinking and washing were critical for system success and maintaining cell viability, as compared to batch photocrosslinking [92]. Our recently published work showed successful hiPSC encapsulation and differentiation within PEG-fibrinogen and GelMA hydrogels to produce 3D-dhECT microislands [23, 24]. In these studies, a 1 mm wide ring of dense cardiac tissue consistently formed around the edge of the microislands. Based on this finding, the desired initial microsphere diameter was chosen to be approximately 1 mm, and thus the resulting sphere diameter using our microfluidic system was 908 μm (n=485 microspheres, 8 individual batches); however, this microfluidic system enables modulation of size and shape, as well as initial cell seeding density, and ongoing studies are investigating the impact of these parameters on resulting cardiac tissue formation. The tight control demonstrated here over size and shape of microsphere tissues both within a batch and between batches is critical for cell production and downstream applications.

In this study, we used a custom microfluidic system to rapidly encapsulate hiPSCs within a clinically relevant biomaterial, PEG-fibrinogen, to produce uniform microspheres in size and shape with high cell viability and maintained proliferative and pluripotent phenotype. Remodeling their PEG-fibrinogen microenvironment, these hiPSC microspheres were subsequently differentiated into functional engineered cardiac tissue microspheres with high CM yield that responded appropriately to outside electrical and pharmacological stimuli and could be maintained

in culture long-term with maintenance of spontaneous contraction (over 3 years, **Supplementary Movie 7**). The microspheres were cultured in static suspension conditions; however, a bioreactor or similar dynamic culture system could be used to improve mass transfer and scale-up production [11]. This microfluidic system has the potential to be leveraged in combination with a bioreactor system for scalable hiPSC differentiation by parallelization of PDMS devices for increased production in order to obtain commercially relevant numbers of engineered cardiac tissues for clinical translation and high-throughput drug testing applications.

Acknowledgements

This work was funded by the National Science Foundation (NSF-CBET-1150854) (P.K., W.J.S., F.B.F., Y.T., E.A.L.) and (NSF-CBET-1743445) (F.B.F., E.A.L.), the American Heart Association (AM HEART-14SDG18610002) (W.J.S., Y.T., and E.A.L.), the Department of Education GAANN (#P200A150075) (M.E.E), an AU-CMB/EPSCoR Summer Fellowship (P.K.), the Alabama EPSCoR Graduate Research Scholarship Program (P.K., F.B.F., Y.T.), and a NSF Graduate Research Fellowship (F.B.F.). Research reported in this publication was supported by the National Center for Advancing Translational Sciences of the National Institutes of Health under award number UL1TR003096 (M.E.E). The content is solely the responsibility of the authors and does not necessarily represent the official views of the National Institutes of Health. The authors would like to thank Dr. Joseph C. Wu MD, PhD at the Stanford Cardiovascular Institute for providing the hiPSC line, SCVI55, and Dr. Lior Gepstein at Technion – Israel Institute of Technology for providing the hiPSC line, Un-Arc 16 Facs II. The authors would also like to thank Michaela Bush for providing assistance with optical mapping analysis, Dr. Joonyul Kim for technical assistance with qPCR, Dr. Vishnu Suppiramaniam and Jenna Bloemer for assistance with the MEA, Dr. Doug Martin for use of the cryostat, Shelly Aono for assistance with Masson's trichrome staining, and the Ethier laboratory at Georgia Tech for providing access to the MicroSquisher.

Author Contributions

P.K., W.S., F.B.F., Y.T., and E.A.L. conceptualized the study; P.K., W.S., F.B.F., and Y.T. developed the methodology. P.K., W.S., F.B.F., Y.T., M.E.E., and E.A.L. performed the experiments and analyzed the data. F.B.F., P.K., W.S., Y.T., M.E.E., and E.A.L. wrote and edited the manuscript. E.A.L provided supervision and funding acquisition.

Competing interests

Auburn University holds two patents related to the cardiac differentiation approach used here and one patent application has been submitted for the microfluidic cell encapsulation system employed. 1. P Kerscher*, AJ Hodge*, EA Lipke, "Encapsulation and Cardiac Differentiation of hiPSCs in 3D PEG-Fibrinogen Hydrogels." U.S. Patent No. 9,587,221, Issued 3/7/2017. 2. P Kerscher*, AJ Hodge*, EA Lipke, "Encapsulation and Cardiac Differentiation of hiPSCs in 3D PEG-Fibrinogen Hydrogels." Continuation, U.S. Patent No. 10301597, Issued 05/28/2019. 3. EA Lipke, Y Tian*, WJ Seeto*, "Microfluidics Device for Fabrication of Large, Uniform, Injectable Hydrogel Microspheres for Cell Encapsulation." Provisional Patent 62/568,652, filed 10/6/2017. US Patent Application No. 16/153,095, filed 10/5/2018, published, pending.

Additional information

Correspondence and requests for materials should be addressed to E.A.L.

Data Availability

The raw data required to reproduce these findings are available upon request.

References

[1] J.C. Del Alamo, D. Lemons, R. Serrano, A. Savchenko, F. Cerignoli, R. Bodmer, M. Mercola, High throughput physiological screening of iPSC-derived cardiomyocytes for drug development, Biochim Biophys Acta 1863(7 Pt B) (2016) 1717-27.
[2] Y. Zhang, J. Mignone, W.R. MacLellan, Cardiac Regeneration and Stem Cells, Physiol Rev 95(4) (2015) 1189-204.
[3] K.R. Stevens, C.E. Murry, Human Pluripotent Stem Cell-Derived Engineered Tissues: Clinical Considerations, Cell Stem Cell 22(3) (2018) 294-297.
[4] J.K. Gwathmey, K. Tsaioun, R.J. Hajjar, Cardionomics: a new integrative approach for screening cardiotoxicity of drug candidates, Expert Opin Drug Metab Toxicol 5(6) (2009) 647-60.
[5] D. Rajamohan, E. Matsa, S. Kalra, J. Crutchley, A. Patel, V. George, C. Denning, Current status of drug screening and disease modelling in human pluripotent stem cells, Bioessays 35(3) (2013) 281-98.
[6] K. Takahashi, K. Tanabe, M. Ohnuki, M. Narita, T. Ichisaka, K. Tomoda, S. Yamanaka, Induction of pluripotent stem cells from adult human fibroblasts by defined factors, Cell 131(5) (2007) 861-72.
[7] P.W. Burridge, E. Matsa, P. Shukla, Z.C. Lin, J.M. Churko, A.D. Ebert, F. Lan, S. Diecke, B. Huber, N.M. Mordwinkin, J.R. Plews, O.J. Abilez, B. Cui, J.D. Gold, J.C. Wu, Chemically defined generation of human cardiomyocytes, Nat Methods 11(8) (2014) 855-60.
[8] X. Lian, J. Zhang, S.M. Azarin, K. Zhu, L.B. Hazeltine, X. Bao, C. Hsiao, T.J. Kamp, S.P. Palecek, Directed cardiomyocyte differentiation from human pluripotent stem cells by modulating Wnt/β-catenin signaling under fully defined conditions, Nat Protoc 8(1) (2013) 162-75.
[9] H. Kempf, B. Andree, R. Zweigerdt, Large-scale production of human pluripotent stem cell derived cardiomyocytes, Advanced Drug Delivery Reviews 96 (2016) 18-30.
[10] H. Fonoudi, H. Ansari, S. Abbasalizadeh, M.R. Larijani, S. Kiani, S. Hashemizadeh, A.S. Zarchi, A. Bosman, G.M. Blue, S. Pahlavan, M. Perry, Y. Orr, Y. Mayorchak, J. Vandenberg, M. Talkhabi, D.S. Winlaw, R.P. Harvey, N. Aghdami, H. Baharvand, A Universal and Robust Integrated Platform for the Scalable Production of Human Cardiomyocytes From Pluripotent Stem Cells, Stem Cells Transl Med 4(12) (2015) 1482-94.
[11] H. Kempf, R. Olmer, C. Kropp, M. Ruckert, M. Jara-Avaca, D. Robles-Diaz, A. Franke, D.A. Elliott, D. Wojciechowski, M. Fischer, A. Roa Lara, G. Kensah, I. Gruh, A. Haverich, U. Martin, R. Zweigerdt, Controlling expansion and cardiomyogenic differentiation of human pluripotent stem cells in scalable suspension culture, Stem Cell Reports 3(6) (2014) 1132-46.
[12] C. Halloin, K. Schwanke, W. Lobel, A. Franke, M. Szepes, S. Biswanath, S. Wunderlich, S. Merkert, N. Weber, F. Osten, J. de la Roche, F. Polten, K. Wollert, T. Kraft, M. Fischer, U. Martin, I. Gruh, H. Kempf, R. Zweigerdt, Continuous WNT Control Enables Advanced hPSC Cardiac Processing and

Prognostic Surface Marker Identification in Chemically Defined Suspension Culture, Stem Cell Reports (2019).
[13] K. Rajala, M. Pekkanen-Mattila, K. Aalto-Setala, Cardiac differentiation of pluripotent stem cells, Stem Cells Int 2011 (2011) 383709.
[14] I. Kehat, D. Kenyagin-Karsenti, M. Snir, H. Segev, M. Amit, A. Gepstein, E. Livne, O. Binah, J. Itskovitz-Eldor, L. Gepstein, Human embryonic stem cells can differentiate into myocytes with structural and functional properties of cardiomyocytes, Journal of Clinical Investigation 108(3) (2001) 407-414.
[15] P.W. Burridge, D. Anderson, H. Priddle, M.D. Barbadillo Munoz, S. Chamberlain, C. Allegrucci, L.E. Young, C. Denning, Improved human embryonic stem cell embryoid body homogeneity and cardiomyocyte differentiation from a novel V-96 plate aggregation system highlights interline variability, Stem Cells 25(4) (2007) 929-38.
[16] K. Osafune, L. Caron, M. Borowiak, R.J. Martinez, C.S. Fitz-Gerald, Y. Sato, C.A. Cowan, K.R. Chien, D.A. Melton, Marked differences in differentiation propensity among human embryonic stem cell lines, Nat Biotechnol 26(3) (2008) 313-5.
[17] M.A. Laflamme, K.Y. Chen, A.V. Naumova, V. Muskheli, J.A. Fugate, S.K. Dupras, H. Reinecke, C. Xu, M. Hassanipour, S. Police, C. O'Sullivan, L. Collins, Y. Chen, E. Minami, E.A. Gill, S. Ueno, C. Yuan, J. Gold, C.E. Murry, Cardiomyocytes derived from human embryonic stem cells in pro-survival factors enhance function of infarcted rat hearts, Nat Biotechnol 25(9) (2007) 1015-24.
[18] L.D. Huyer, M. Montgomery, Y. Zhao, Y. Xiao, G. Conant, A. Korolj, M. Radisic, Biomaterial based cardiac tissue engineering and its applications, Biomed Mater 10(3) (2015) 034004.
[19] N. Landa, L. Miller, M.S. Feinberg, R. Holbova, M. Shachar, I. Freeman, S. Cohen, J. Leor, Effect of injectable alginate implant on cardiac remodeling and function after recent and old infarcts in rat, Circulation 117(11) (2008) 1388-96.
[20] B. Abecasis, P.G.M. Canhao, H.V. Almeida, T. Calmeiro, E. Fortunato, P. Gomes-Alves, M. Serra, P.M. Alves, Toward a Microencapsulated 3D hiPSC-Derived in vitro Cardiac Microtissue for Recapitulation of Human Heart Microenvironment Features, Front Bioeng Biotechnol 8 (2020) 580744.
[21] J.S. Wendel, L. Ye, P. Zhang, R.T. Tranquillo, J.J. Zhang, Functional consequences of a tissue-engineered myocardial patch for cardiac repair in a rat infarct model, Tissue Eng Part A 20(7-8) (2014) 1325-35.
[22] D.A. Dunn, A.J. Hodge, E.A. Lipke, Biomimetic materials design for cardiac tissue regeneration, Wiley Interdiscip Rev Nanomed Nanobiotechnol 6(1) (2014) 15-39.
[23] P. Kerscher, I.C. Turnbull, A.J. Hodge, J. Kim, D. Seliktar, C.J. Easley, K.D. Costa, E.A. Lipke, Direct hydrogel encapsulation of pluripotent stem cells enables ontomimetic differentiation and growth of engineered human heart tissues, Biomaterials 83 (2016) 383-95.
[24] P. Kerscher, J.A. Kaczmarek, S.E. Head, M.E. Ellis, W.J. Seeto, J. Kim, S. Bhattacharya, V. Suppiramaniam, E.A. Lipke, Direct Production of Human Cardiac Tissues by Pluripotent Stem Cell Encapsulation in Gelatin Methacryloyl, ACS Biomaterials Science & Engineering 3(8) (2016) 1499-1509.
[25] L. Almany, D. Seliktar, Biosynthetic hydrogel scaffolds made from fibrinogen and polyethylene glycol for 3D cell cultures, Biomaterials 26(15) (2005) 2467-77.
[26] M.J. Jenkins, S.S. Farid, Human pluripotent stem cell-derived products: advances towards robust, scalable and cost-effective manufacturing strategies, Biotechnol J 10(1) (2015) 83-95.
[27] S. Trattnig, K. Ohel, V. Mlynarik, V. Juras, S. Zbyn, A. Korner, Morphological and compositional monitoring of a new cell-free cartilage repair hydrogel technology - GelrinC by MR using semi-quantitative MOCART scoring and quantitative T2 index and new zonal T2 index calculation, Osteoarthritis Cartilage 23(12) (2015) 2224-2232.
[28] R. Shinnawi, I. Huber, L. Maizels, N. Shaheen, A. Gepstein, G. Arbel, A.J. Tijsen, L. Gepstein, Monitoring Human-Induced Pluripotent Stem Cell-Derived Cardiomyocytes with Genetically Encoded Calcium and Voltage Fluorescent Reporters, Stem Cell Reports 5(4) (2015) 582-96.
[29] S.A. DeLong, J.J. Moon, J.L. West, Covalently immobilized gradients of bFGF on hydrogel scaffolds for directed cell migration, Biomaterials 26(16) (2005) 3227-34.

[30] D. Dikovsky, H. Bianco-Peled, D. Seliktar, The effect of structural alterations of PEG-fibrinogen hydrogel scaffolds on 3-D cellular morphology and cellular migration, Biomaterials 27(8) (2006) 1496-506.
[31] M.A. Kinney, T.A. Hookway, Y. Wang, T.C. McDevitt, Engineering three-dimensional stem cell morphogenesis for the development of tissue models and scalable regenerative therapeutics, Ann Biomed Eng 42(2) (2014) 352-67.
[32] K. Kim, J. Cheng, Q. Liu, X.Y. Wu, Y. Sun, Investigation of mechanical properties of soft hydrogel microcapsules in relation to protein delivery using a MEMS force sensor, J Biomed Mater Res A 92(1) (2010) 103-13.
[33] A.J. Hodge, J. Zhong, E.A. Lipke, Enhanced stem cell-derived cardiomyocyte differentiation in suspension culture by delivery of nitric oxide using S-nitrosocysteine, Biotechnol Bioeng 113(4) (2016) 882-94.
[34] W.J. Seeto, Y. Tian, R.L. Winter, F.J. Caldwell, A.A. Wooldridge, E.A. Lipke, Encapsulation of Equine Endothelial Colony Forming Cells in Highly Uniform, Injectable Hydrogel Microspheres for Local Cell Delivery, Tissue engineering. Part C, Methods 23(11) (2017) 815-825.
[35] X. Lian, C. Hsiao, G. Wilson, K. Zhu, L.B. Hazeltine, S.M. Azarin, K.K. Raval, J. Zhang, T.J. Kamp, S.P. Palecek, Robust cardiomyocyte differentiation from human pluripotent stem cells via temporal modulation of canonical Wnt signaling, Proc Natl Acad Sci U S A 109(27) (2012) E1848-57.
[36] I.Y. Shadrin, B.W. Allen, Y. Qian, C.P. Jackman, A.L. Carlson, M.E. Juhas, N. Bursac, Cardiopatch platform enables maturation and scale-up of human pluripotent stem cell-derived engineered heart tissues, Nat Commun 8(1) (2017) 1825.
[37] R. Saunders, M. Amoroso, SEM investigation of heart tissue samples, Journal of Physics: Conference Series 241 (2010) 012023.
[38] N.T. Feric, M. Radisic, Maturing human pluripotent stem cell-derived cardiomyocytes in human engineered cardiac tissues, Adv Drug Deliv Rev 96 (2016) 110-34.
[39] N. Huebsch, P. Loskill, M.A. Mandegar, N.C. Marks, A.S. Sheehan, Z. Ma, A. Mathur, T.N. Nguyen, J.C. Yoo, L.M. Judge, C.I. Spencer, A.C. Chukka, C.R. Russell, P.L. So, B.R. Conklin, K.E. Healy, Automated Video-Based Analysis of Contractility and Calcium Flux in Human-Induced Pluripotent Stem Cell-Derived Cardiomyocytes Cultured over Different Spatial Scales, Tissue engineering. Part C, Methods 21(5) (2015) 467-79.
[40] A.M. Bratt-Leal, R.L. Carpenedo, T.C. McDevitt, Engineering the embryoid body microenvironment to direct embryonic stem cell differentiation, Biotechnol Prog 25(1) (2009) 43-51.
[41] G. Pettinato, X. Wen, N. Zhang, Formation of well-defined embryoid bodies from dissociated human induced pluripotent stem cells using microfabricated cell-repellent microwell arrays, Sci Rep 4 (2014) 7402.
[42] M.A. Branco, J.P. Cotovio, C.A.V. Rodrigues, S.H. Vaz, T.G. Fernandes, L.M. Moreira, J.M.S. Cabral, M.M. Diogo, Transcriptomic analysis of 3D Cardiac Differentiation of Human Induced Pluripotent Stem Cells Reveals Faster Cardiomyocyte Maturation Compared to 2D Culture, Sci Rep 9(1) (2019) 9229.
[43] E.S. Ng, R.P. Davis, L. Azzola, E.G. Stanley, A.G. Elefanty, Forced aggregation of defined numbers of human embryonic stem cells into embryoid bodies fosters robust, reproducible hematopoietic differentiation, Blood 106(5) (2005) 1601-3.
[44] M.D. Ungrin, C. Joshi, A. Nica, C. Bauwens, P.W. Zandstra, Reproducible, ultra high-throughput formation of multicellular organization from single cell suspension-derived human embryonic stem cell aggregates, Plos One 3(2) (2008) e1565.
[45] P. Beauchamp, W. Moritz, J.M. Kelm, N.D. Ullrich, I. Agarkova, B.D. Anson, T.M. Suter, C. Zuppinger, Development and Characterization of a Scaffold-Free 3D Spheroid Model of Induced Pluripotent Stem Cell-Derived Human Cardiomyocytes, Tissue engineering. Part C, Methods 21(8) (2015) 852-61.
[46] S. Pradhan, J.M. Clary, D. Seliktar, E.A. Lipke, A three-dimensional spheroidal cancer model based on PEG-fibrinogen hydrogel microspheres, Biomaterials 115 (2017) 141-154.

[47] D. Jing, A. Parikh, E.S. Tzanakakis, Cardiac cell generation from encapsulated embryonic stem cells in static and scalable culture systems, Cell Transplant 19(11) (2010) 1397-412.
[48] L.R. Madden, D.J. Mortisen, E.M. Sussman, S.K. Dupras, J.A. Fugate, J.L. Cuy, K.D. Hauch, M.A. Laflamme, C.E. Murry, B.D. Ratner, Proangiogenic scaffolds as functional templates for cardiac tissue engineering, Proc Natl Acad Sci U S A 107(34) (2010) 15211-6.
[49] N.L. Tulloch, V. Muskheli, M.V. Razumova, F.S. Korte, M. Regnier, K.D. Hauch, L. Pabon, H. Reinecke, C.E. Murry, Growth of engineered human myocardium with mechanical loading and vascular coculture, Circ Res 109(1) (2011) 47-59.
[50] L.A. Reis, L.L. Chiu, N. Feric, L. Fu, M. Radisic, Biomaterials in myocardial tissue engineering, J Tissue Eng Regen Med 10(1) (2016) 11-28.
[51] M. Habib, K. Shapira-Schweitzer, O. Caspi, A. Gepstein, G. Arbel, D. Aronson, D. Seliktar, L. Gepstein, A combined cell therapy and in-situ tissue-engineering approach for myocardial repair, Biomaterials 32(30) (2011) 7514-23.
[52] Y. Shao, J. Sang, J. Fu, On human pluripotent stem cell control: The rise of 3D bioengineering and mechanobiology, Biomaterials 52 (2015) 26-43.
[53] J.P. Guyette, J.M. Charest, R.W. Mills, B.J. Jank, P.T. Moser, S.E. Gilpin, J.R. Gershlak, T. Okamoto, G. Gonzalez, D.J. Milan, G.R. Gaudette, H.C. Ott, Bioengineering Human Myocardium on Native Extracellular Matrix, Circ Res 118(1) (2016) 56-72.
[54] A.M. Bratt-Leal, R.L. Carpenedo, M.D. Ungrin, P.W. Zandstra, T.C. McDevitt, Incorporation of biomaterials in multicellular aggregates modulates pluripotent stem cell differentiation, Biomaterials 32(1) (2011) 48-56.
[55] B.S. Spearman, A.J. Hodge, J.L. Porter, J.G. Hardy, Z.D. Davis, T. Xu, X. Zhang, C.E. Schmidt, M.C. Hamilton, E.A. Lipke, Conductive interpenetrating networks of polypyrrole and polycaprolactone encourage electrophysiological development of cardiac cells, Acta Biomater 28 (2015) 109-120.
[56] S.R. Shin, S.M. Jung, M. Zalabany, K. Kim, P. Zorlutuna, S.B. Kim, M. Nikkhah, M. Khabiry, M. Azize, J. Kong, K.T. Wan, T. Palacios, M.R. Dokmeci, H. Bae, X.S. Tang, A. Khademhosseini, Carbon-nanotube-embedded hydrogel sheets for engineering cardiac constructs and bioactuators, ACS Nano 7(3) (2013) 2369-80.
[57] A. Paul, A. Hasan, H.A. Kindi, A.K. Gaharwar, V.T. Rao, M. Nikkhah, S.R. Shin, D. Krafft, M.R. Dokmeci, D. Shum-Tim, A. Khademhosseini, Injectable graphene oxide/hydrogel-based angiogenic gene delivery system for vasculogenesis and cardiac repair, ACS Nano 8(8) (2014) 8050-62.
[58] D.H. Kim, E.A. Lipke, P. Kim, R. Cheong, S. Thompson, M. Delannoy, K.Y. Suh, L. Tung, A. Levchenko, Nanoscale cues regulate the structure and function of macroscopic cardiac tissue constructs, Proc Natl Acad Sci U S A 107(2) (2010) 565-70.
[59] S. Sugiura, J.M. Cha, F. Yanagawa, P. Zorlutuna, H. Bae, A. Khademhosseini, Dynamic three-dimensional micropatterned cell co-cultures within photocurable and chemically degradable hydrogels, J Tissue Eng Regen Med 10(8) (2016) 690-9.
[60] S.S. Nunes, J.W. Miklas, J. Liu, R. Aschar-Sobbi, Y. Xiao, B. Zhang, J. Jiang, S. Masse, M. Gagliardi, A. Hsieh, N. Thavandiran, M.A. Laflamme, K. Nanthakumar, G.J. Gross, P.H. Backx, G. Keller, M. Radisic, Biowire: a platform for maturation of human pluripotent stem cell-derived cardiomyocytes, Nat Methods 10(8) (2013) 781-7.
[61] K. Ronaldson-Bouchard, S.P. Ma, K. Yeager, T. Chen, L. Song, D. Sirabella, K. Morikawa, D. Teles, M. Yazawa, G. Vunjak-Novakovic, Advanced maturation of human cardiac tissue grown from pluripotent stem cells, Nature 556(7700) (2018) 239-243.
[62] J.L. Young, A.J. Engler, Hydrogels with time-dependent material properties enhance cardiomyocyte differentiation in vitro, Biomaterials 32(4) (2011) 1002-9.
[63] L.B. Hazeltine, M.G. Badur, X. Lian, A. Das, W. Han, S.P. Palecek, Temporal impact of substrate mechanics on differentiation of human embryonic stem cells to cardiomyocytes, Acta Biomater 10(2) (2014) 604-12.
[64] L. Davidson, R. Keller, Measuring Mechanical Properties of Embryos and Embryonic Tissues, 83 (2007) 425-439.

[65] N. Ferri, P. Siegl, A. Corsini, J. Herrmann, A. Lerman, R. Benghozi, Drug attrition during pre-clinical and clinical development: understanding and managing drug-induced cardiotoxicity, Pharmacol Ther 138(3) (2013) 470-84.
[66] B. Fermini, S.T. Coyne, K.P. Coyne, Clinical Trials in a Dish: A Perspective on the Coming Revolution in Drug Development, SLAS Discov 23(8) (2018) 765-776.
[67] P.W. Burridge, S. Thompson, M.A. Millrod, S. Weinberg, X. Yuan, A. Peters, V. Mahairaki, V.E. Koliatsos, L. Tung, E.T. Zambidis, A universal system for highly efficient cardiac differentiation of human induced pluripotent stem cells that eliminates interline variability, PLoS One 6(4) (2011) e18293.
[68] J.M. Pioner, L. Santini, C. Palandri, D. Martella, F. Lupi, M. Langione, S. Querceto, B. Grandinetti, V. Balducci, P. Benzoni, S. Landi, A. Barbuti, F. Ferrarese Lupi, L. Boarino, L. Sartiani, C. Tesi, D.L. Mack, M. Regnier, E. Cerbai, C. Parmeggiani, C. Poggesi, C. Ferrantini, R. Coppini, Optical Investigation of Action Potential and Calcium Handling Maturation of hiPSC-Cardiomyocytes on Biomimetic Substrates, Int J Mol Sci 20(15) (2019).
[69] C.W. Don, C.E. Murry, Improving survival and efficacy of pluripotent stem cell-derived cardiac grafts, J Cell Mol Med 17(11) (2013) 1355-62.
[70] K.A. Gerbin, X. Yang, C.E. Murry, K.L. Coulombe, Enhanced Electrical Integration of Engineered Human Myocardium via Intramyocardial versus Epicardial Delivery in Infarcted Rat Hearts, PLoS One 10(7) (2015) e0131446.
[71] L. Carpenter, C. Carr, C.T. Yang, D.J. Stuckey, K. Clarke, S.M. Watt, Efficient differentiation of human induced pluripotent stem cells generates cardiac cells that provide protection following myocardial infarction in the rat, Stem Cells Dev 21(6) (2012) 977-86.
[72] J.J. Chong, X. Yang, C.W. Don, E. Minami, Y.W. Liu, J.J. Weyers, W.M. Mahoney, B. Van Biber, S.M. Cook, N.J. Palpant, J.A. Gantz, J.A. Fugate, V. Muskheli, G.M. Gough, K.W. Vogel, C.A. Astley, C.E. Hotchkiss, A. Baldessari, L. Pabon, H. Reinecke, E.A. Gill, V. Nelson, H.P. Kiem, M.A. Laflamme, C.E. Murry, Human embryonic-stem-cell-derived cardiomyocytes regenerate non-human primate hearts, Nature 510(7504) (2014) 273-7.
[73] S.D. Lundy, J.A. Gantz, C.M. Pagan, D. Filice, M.A. Laflamme, Pluripotent stem cell derived cardiomyocytes for cardiac repair, Curr Treat Options Cardiovasc Med 16(7) (2014) 319.
[74] M. Mirotsou, T.M. Jayawardena, J. Schmeckpeper, M. Gnecchi, V.J. Dzau, Paracrine mechanisms of stem cell reparative and regenerative actions in the heart, Journal of Molecular and Cellular Cardiology 50(2) (2011) 280-289.
[75] C.P. Hodgkinson, A. Bareja, J.A. Gomez, V.J. Dzau, Emerging Concepts in Paracrine Mechanisms in Regenerative Cardiovascular Medicine and Biology, Circ Res 118(1) (2016) 95-107.
[76] G. Blin, D. Nury, S. Stefanovic, T. Neri, O. Guillevic, B. Brinon, V. Bellamy, C. Rucker-Martin, P. Barbry, A. Bel, P. Bruneval, C. Cowan, J. Pouly, S. Mitalipov, E. Gouadon, P. Binder, A. Hagege, M. Desnos, J.F. Renaud, P. Menasche, M. Puceat, A purified population of multipotent cardiovascular progenitors derived from primate pluripotent stem cells engrafts in postmyocardial infarcted nonhuman primates, J Clin Invest 120(4) (2010) 1125-39.
[77] V. Bellamy, V. Vanneaux, A. Bel, H. Nemetalla, S. Emmanuelle Boitard, Y. Farouz, P. Joanne, M.C. Perier, E. Robidel, C. Mandet, A. Hagege, P. Bruneval, J. Larghero, O. Agbulut, P. Menasche, Long-term functional benefits of human embryonic stem cell-derived cardiac progenitors embedded into a fibrin scaffold, J Heart Lung Transplant 34(9) (2015) 1198-207.
[78] P. Joanne, M. Kitsara, S.E. Boitard, H. Naemetalla, V. Vanneaux, M. Pernot, J. Larghero, P. Forest, Y. Chen, P. Menasche, O. Agbulut, Nanofibrous clinical-grade collagen scaffolds seeded with human cardiomyocytes induces cardiac remodeling in dilated cardiomyopathy, Biomaterials 80 (2016) 157-68.
[79] P. Menasche, V. Vanneaux, A. Hagege, A. Bel, B. Cholley, A. Parouchev, I. Cacciapuoti, R. Al-Daccak, N. Benhamouda, H. Blons, O. Agbulut, L. Tosca, J.H. Trouvin, J.R. Fabreguettes, V. Bellamy, D. Charron, E. Tartour, G. Tachdjian, M. Desnos, J. Larghero, Transplantation of Human Embryonic Stem Cell-Derived Cardiovascular Progenitors for Severe Ischemic Left Ventricular Dysfunction, J Am Coll Cardiol 71(4) (2018) 429-438.

[80] P. Menasche, Cell therapy trials for heart regeneration - lessons learned and future directions, Nat Rev Cardiol 15(11) (2018) 659-671.
[81] S. El-Kirat-Chatel, A. Beaussart, S.P. Vincent, M. Abellan Flos, P. Hols, P.N. Lipke, Y.F. Dufrene, Forces in yeast flocculation, Nanoscale 7(5) (2015) 1760-7.
[82] H.W. Kang, S.J. Lee, I.K. Ko, C. Kengla, J.J. Yoo, A. Atala, A 3D bioprinting system to produce human-scale tissue constructs with structural integrity, Nat Biotechnol 34(3) (2016) 312-9.
[83] L. Ouyang, R. Yao, S. Mao, X. Chen, J. Na, W. Sun, Three-dimensional bioprinting of embryonic stem cells directs highly uniform embryoid body formation, Biofabrication 7(4) (2015) 044101.
[84] Y. Ma, Y. Ji, G. Huang, K. Ling, X. Zhang, F. Xu, Bioprinting 3D cell-laden hydrogel microarray for screening human periodontal ligament stem cell response to extracellular matrix, Biofabrication 7(4) (2015) 044105.
[85] M.E. Kupfer, W.H. Lin, V. Ravikumar, K. Qiu, L. Wang, L. Gao, D. Bhuiyan, M. Lenz, J. Ai, R.R. Mahutga, D. Townsend, J. Zhang, M.C. McAlpine, E.G. Tolkacheva, B.M. Ogle, In Situ Expansion, Differentiation and Electromechanical Coupling of Human Cardiac Muscle in a 3D Bioprinted, Chambered Organoid, Circ Res (2020).
[86] H.F. Chan, Y. Zhang, K.W. Leong, Efficient One-Step Production of Microencapsulated Hepatocyte Spheroids with Enhanced Functions, Small (2016).
[87] X. Zhao, S. Liu, L. Yildirimer, H. Zhao, R. Ding, H. Wang, W. Cui, D. Weitz, Injectable Stem Cell-Laden Photocrosslinkable Microspheres Fabricated Using Microfluidics for Rapid Generation of Osteogenic Tissue Constructs, Adv Funct Mater (2016) n/a-n/a.
[88] Z. Jiang, B. Xia, R. McBride, J. Oakey, A microfluidic-based cell encapsulation platform to achieve high long-term cell viability in photopolymerized PEGNB hydrogel microspheres, J Mater Chem B Mater Biol Med 5(1) (2017) 173-180.
[89] I. Gal, R. Edri, N. Noor, M. Rotenberg, M. Namestnikov, I. Cabilly, A. Shapira, T. Dvir, Injectable Cardiac Cell Microdroplets for Tissue Regeneration, Small (2020) e1904806.
[90] T. Rossow, P.S. Lienemann, D.J. Mooney, Cell Microencapsulation by Droplet Microfluidic Templating, Macromolecular Chemistry and Physics 218(2) (2017) 1600380.
[91] W.J. Seeto, Y. Tian, S. Pradhan, P. Kerscher, E.A. Lipke, Rapid Production of Cell-Laden Microspheres Using a Flexible Microfluidic Encapsulation Platform, Small 15(47) (2019) e1902058.
[92] S. Chang, F. Finklea, B. Williams, H. Hammons, A. Hodge, S. Scott, E. Lipke, Emulsion-based Encapsulation of Pluripotent Stem Cells in Hydrogel Microspheres for Cardiac Differentiation, Biotechnol Prog (2020).

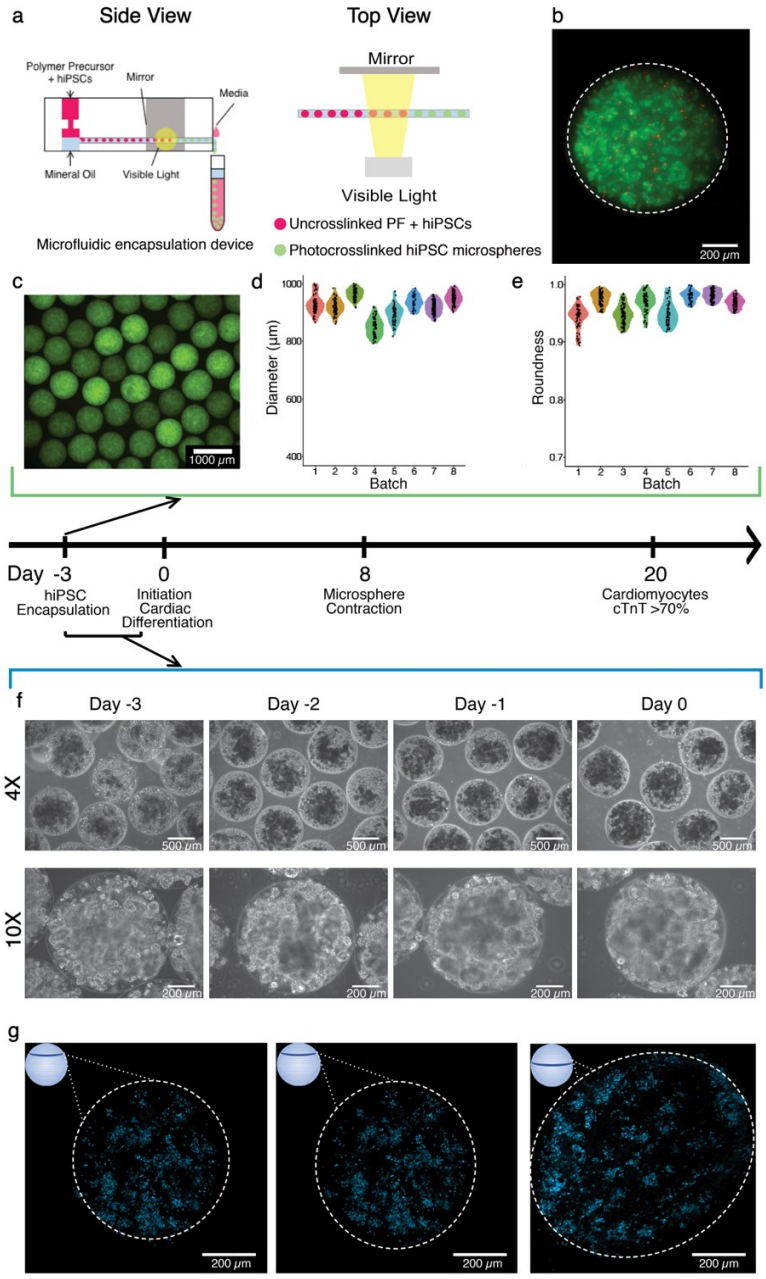

Figure 1. Rapid, highly reproducible hiPSC-encapsulation process to produce uniform cardiac tissue microspheres. (a) HiPSCs suspended in aqueous hydrogel precursor solution (25 million cells mL^{-1}, discrete phase) were infused through a custom PDMS mold opposite an oil phase (continuous phase) to produce uniform cell-laden microspheres. Microspheres formed at the junction of the PDMS device and then traveled through the outlet channel where photocrosslinking occurred for 1.6 seconds, resulting in a cell encapsulation rate of 420,000 cells per minute. (b) Encapsulated hiPSCs maintained high cell viability as visualized using a Live/Dead Assay with live cells shown in green and dead cells in red. Dashed white line indicates microsphere perimeter. (c) Microspheres were highly uniform as visualized at 24 *h* post-production using long acquisition times to detect the Eosin Y autofluorescence. (d-e) Microsphere diameter and circularity were

consistent both within a batch and between batches as shown in the violin plots. Each color represents an individual batch while each measured microsphere is represented by a black dot. Microspheres were (d) 908 ± 40 μm in diameter and (e) were highly circular (0.956 ± 0.02) (n = 8 individual batches, 485 spheres analyzed). (f) HiPSCs were successfully encapsulated in microspheres and maintained in suspension culture prior to cardiac differentiation initiation, as visualized here in daily phase contrast images. (g) Cryosections from day 0 show uniform distribution of cells throughout the hydrogel based on number of Hoechst-labeled (blue) nuclei per cross sectional area. Inset schematic shows slice location based on measured diameter.

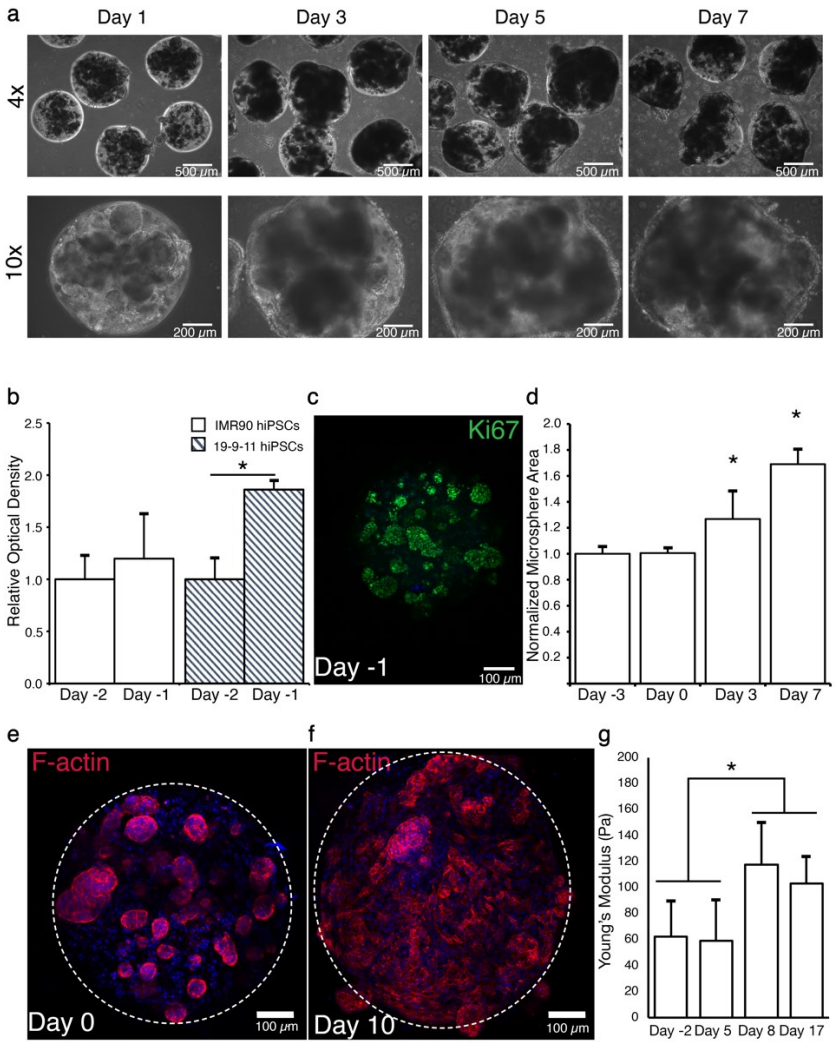

Figure 2. Cell-laden PEG-fibrinogen microspheres grew to form uniform tissues. (a) During differentiation, the cells within the microspheres continued to proliferate and remodel their provided PEG-fibrinogen microenvironment as seen in phase contrast images throughout the time course of cardiac differentiation. (b) Prior to cardiac differentiation, cell proliferation for two hiPSC lines was verified by XTT assay, which showed an increase in optical density between day -2 and day -1 ($n = 5$ microspheres per condition, $*p < 0.05$), indicating continued proliferation and growth of the cells. (c) The hiPSCs maintain their proliferative phenotype following cell encapsulation as shown by positive expression of Ki67 (green) on day -1. (d) From the onset of cardiac differentiation (day 0), microsphere size increased by a factor of 1.27 by day 3 and 1.7 by day 7 ($n = 10$, $*p < 0.05$). (e) Prior to initiation of cardiac differentiation, hiPSCs grew as rounded colonies within the microspheres as visualized on day 0 (3 days post-encapsulation) through labeling of F-actin filaments (red). Dashed white line indicates microsphere perimeter. (f) Following cardiac differentiation, cells are more elongated, indicative of cardiomyocyte phenotype. (g) The PEG-fibrinogen provides an initially soft microenvironment (<250 Pa), and a significant increase in stiffness occurs during cardiac differentiation ($n = 8$ microspheres per condition, $*p < 0.05$).

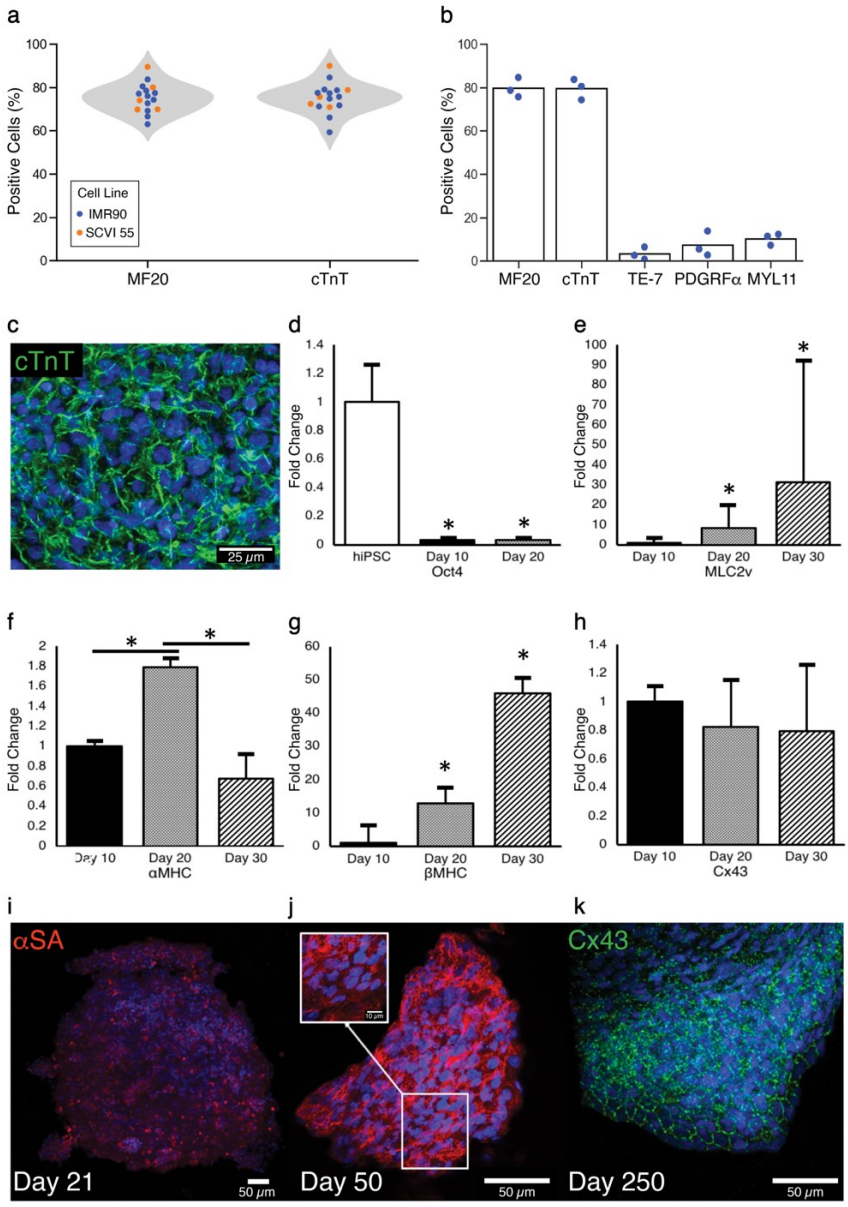

Figure 3. 3D cardiac microsphere differentiation enabled high CM yield and reproducibility between batches with appropriate gene expression. (a) For two different cell lines, IMR90 and SCVI55, 75.2 ± 7.1% and 75.1 ± 6.7% were positive for cardiac markers, MF20 and cTnT, respectively, on day 10 (n = 16 individual batches). Each dot represents an individual batch. (b) Additional cells were primarily fibroblasts and smooth muscle cells, with 3.3 ± 2.9% positive for fibroblast marker, TE-7, 7.36 ± 5.75% positive for cardiac fibroblast marker, PDGFRα, and 10.3 ± 2.7% positive for smooth muscle marker, MYL11. (c) CM morphology and distribution on the surface of a microsphere visualized by positive expression of cTnT (green) and Hoechst (blue) on day 12. (d-h) The resulting engineered cardiac microspheres exhibited appropriate temporal changes in gene expression, including a decrease in pluripotency gene, Oct4, as well as appropriate changes in cardiac genes MLC2v, αMHC, and βMHC. The expression of functional protein Cx43

remained constant between day 10 and day 30. ($n = 3$ biological replicates in duplicate, $*p < 0.05$) (i-j) From day 21 to day 50, the sarcomeres become more aligned, a feature of maturing CMs, shown by positive expression of αSA (red) and Hoechst (blue) within cryosections. (k) Cardiac tissue microspheres express the gap junction protein Cx43 (green, day 250) with nuclei labeled (blue).

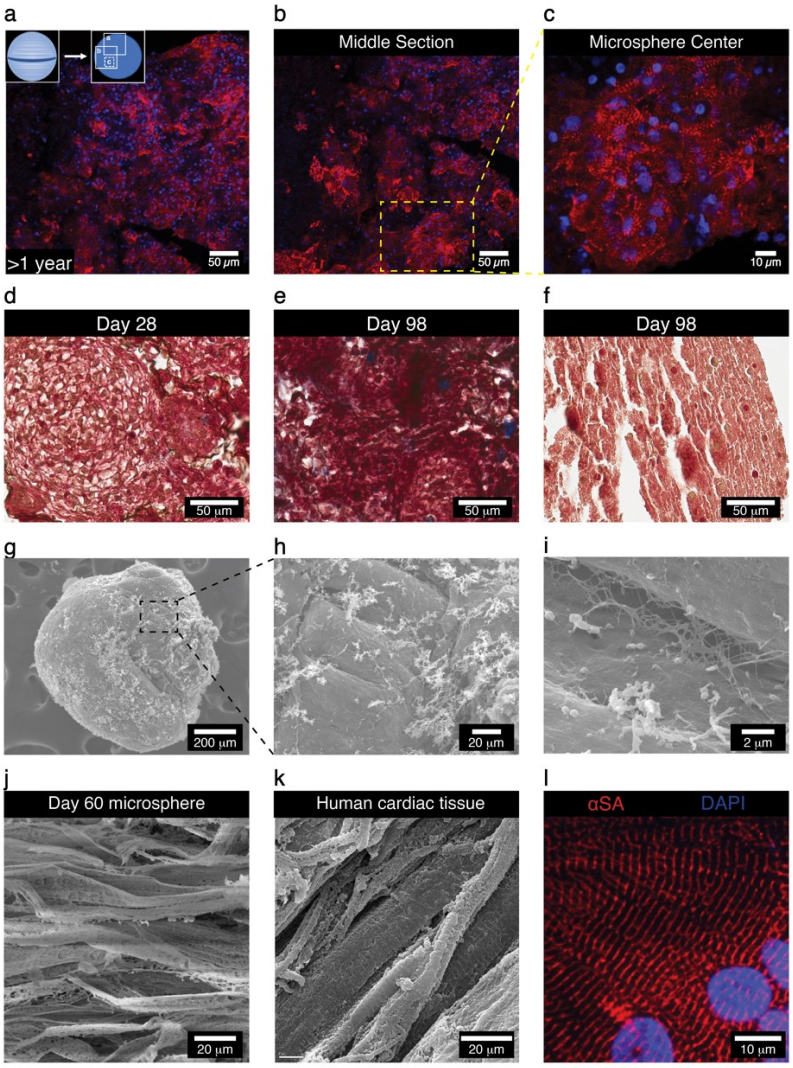

Figure 4. Engineered cardiac tissue microspheres displayed features of maturing cells. Cardiac tissue microspheres were maintained long-term in culture. (a-c) A representative cryosection from the middle of the microsphere showing that cardiac differentiation occurred throughout the entire engineered cardiac microsphere volume (cardiac marker αSA (red), nuclei Hoechst (blue), additional slices **Supplementary Figure 5**). (d-f) As visualized by Masson's trichrome staining, CMs remodeled their microenvironment and deposited ECM; an increasing amount of collagen (blue) was detected during culture time with minimal collagen detected on (d) day 28 with increasing collagen deposition by (e) day 98. (f) ECT microsphere sections on day 98 contained areas of cell alignment and organization similar to native cardiac tissue. Scanning electron microscopy (SEM) images show (g) the cells remodeled their PEG-fibrinogen microenvironment to form dense cardiac tissue microspheres with (h) aligned cells along the edge and ECM deposition on the microsphere surface. (i) At higher magnification, junctions between two adjoining cells could be visualized. (j) Myofibril structure was observed on the edge of day 60 microspheres, similar to (k) human cardiac tissue samples [37] (Figure reprinted with permission). (l) Dissociated CMs show highly aligned sarcomeres (red) indicating progression of CM maturation, as visualized by positive αSA expression.

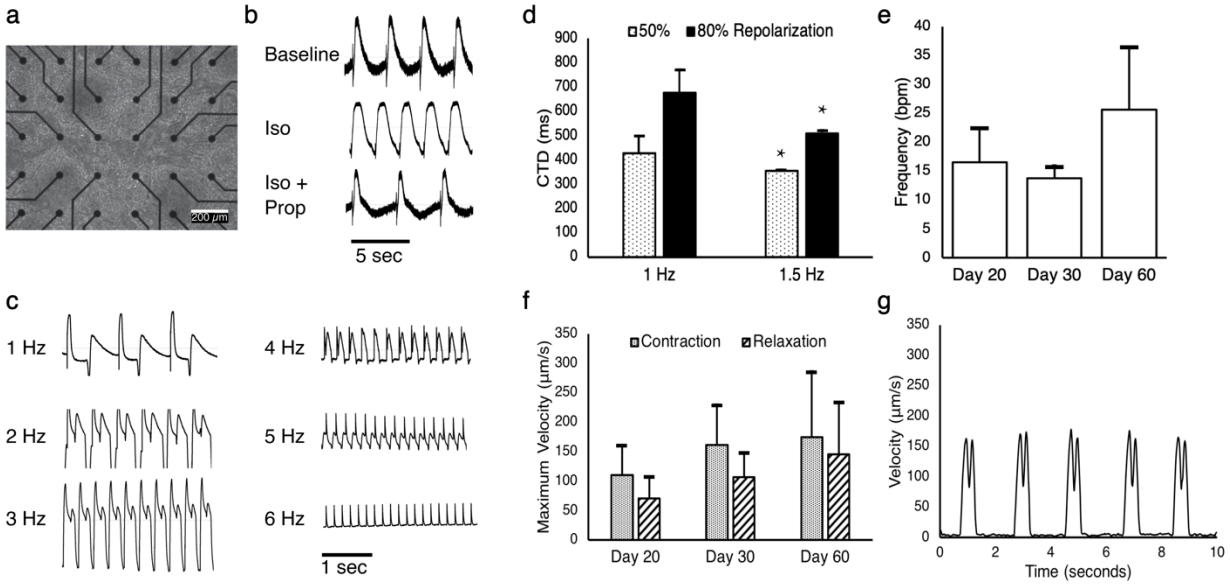

Figure 5. Microsphere CMs responded to pharmacological and electrical stimuli indicating functionality. (a-c) Microspheres were dissociated and plated on the MEA (**Supplementary Movie 6**). (b) Day 20 CMs responded to β-adrenergic agonist, isoproterenol (Iso), increasing the contraction rate. The subsequent addition of propranolol (Prop), a β-adrenergic antagonist, reversed the initial increase in contraction rate caused by isoproterenol. (c) In addition to appropriate response to drug treatment, day 50 microsphere CMs showed 1:1 capture in response to exogenous pacing frequencies up to 6.0 Hz. (d) Optical mapping was used to visualize calcium transients in plated cardiac microspheres tissues (day 74); recordings showed an expected decrease in calcium transient duration (CTD) with increased frequency of electrical pacing (n = minimum 3200 locations, $*p < 0.05$). The CTD was 430 ms and 350 ms for 50% repolarization and 680 ms and 500 ms at 80% repolarization for 1 Hz and 1.5 Hz pacing, respectively. (e) Analysis of engineered cardiac microsphere tissues showed a contraction rate of 16.6 ± 5.9, 13.8 ± 2.3, and 25.6 ± 10.8 beats per minute on days 20, 30, and 60, respectively (n = minimum 11 per condition). (f) Cardiac microsphere contraction velocities were 110±49, 161±69, and 175±112 μm s^{-1} on days 20, 30, and 60 with relaxation velocities of 70 ± 36, 106 ± 42, and 146 ± 88 μm s^{-1}, respectively; a representative trace is shown in (g) (n = minimum 11 samples per condition).